Self-Catalyzed Carbon Dioxide Adsorption by Metal–Organic Chains on Gold Surfaces

Min Feng,[†] Hao Sun,[‡,§] Jin Zhao,[†,‡,§] and Hrvoje Petek[†,*]

[†]Department of Physics and Astronomy, University of Pittsburgh, Pittsburgh, Pennsylvania 15260, United States, [‡]Hefei National Laboratory for Physical Sciences at Microscale and Department of Physics, University of Science and Technology of China, Hefei, Anhui 230026, P.R. China, and [§]Synergetic Innovation Center of Quantum Information & Quantum Physics, University of Science and Technology of China, Hefei, Anhui 230026, China

ABSTRACT Efficient capture of CO_2 by chemical means requires a microscopic understanding of the interactions of the molecule–substrate bonding and adsorption-induced collective phenomena. By molecule-resolved imaging with scanning tunneling microscopy (STM), we investigate self-catalyzed CO_2 adsorption on one-dimensional (1D) substrates composed of self-assembled metal–organic chains (MOCs) supported on gold surfaces. CO_2 adsorption turns on attractive interchain interactions, which induce pronounced surface structural changes; the initially uniformly dispersed chains gather into close packed bundles, which are held together by highly ordered, single molecule wide CO_2 ranks. CO_2 molecules create more favorable adsorption sites for further CO_2 adsorption by mediating the interchain attraction, thereby self-catalyzing their capture. The release of CO_2 molecules by thermal desorption returns the MOCs to their original structure, indicating that the CO_2 capture and release are reversible processes. The real space microscopic characterization of the self-catalyzed CO_2 adsorption on 1D substrates could be exploited as platform for design of molecular materials for CO_2 capture and reduction.

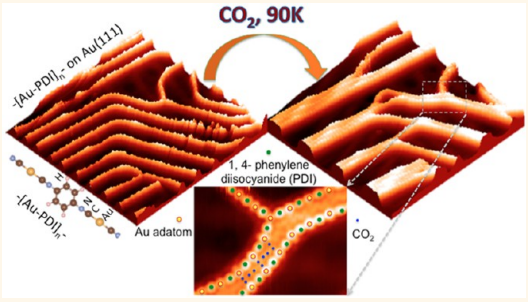

KEYWORDS: self-catalyzed CO_2 adsorption · surface metal–organic chains · 1D substrate · collective phenomena

Environment and energy concerns have aroused intense interest in the chemistry of CO_2.[1−3] An efficient method for the selective CO_2 capture from dilute streams and its reduction into useful hydrocarbon chemicals could impact the carbon economy. Progress in this direction can be made through research on advanced materials that undergo pronounced chemical and physical changes upon exposure to CO_2 molecules. The design of such materials requires a molecular level understanding of CO_2 molecule–substrate interactions and correlated molecular behavior that they might trigger.[4,5] Three-dimensional (3D) metal–organic nanoporous materials, such as metal–organic frameworks (MOFs) and porous coordination polymers (PCPs), have emerged as the promising materials for CO_2 capture because they offer a large surface-to-volume ratios and great versatility in design of guest–host interactions by the selection of the metal and organic components as well as their distribution in space.[5−12] In the case of CO molecule, a recent study showed that weak adsorption of CO at the metal sites within a PCP stimulates marked structural changes of the porous crystal, which create additional favorable sites for further adsorption of CO. This cooperative behavior achieves self-accelerating, highly selective CO capture.[11] Such self-accelerating or self-catalyzed interactions are likely to be useful for the selective capture and chemistry of other molecules such as CO_2, where the substrates can benefit not only from pairwise interactions, but also from cooperative phenomena where the chemical changes brought on by the primary interactions create a more favorable environment for the subsequent adsorption.

Here we report on the self-catalyzed CO_2 capture on gold surfaces functionalized with 1D metal–organic chains (MOCs). 1D surfaces enable strong adsorbate–substrate interactions as well as adsorption-induced cooperative phenomena that are more

* Address correspondence to petek@pitt.edu.

Received for review June 27, 2014 and accepted July 29, 2014.

Published online July 29, 2014
10.1021/nn5035026

pronounced than for the less mutable 2D surfaces.[13] The primary example of 1D surfaces are noble metal−oxygen atom added row structures on Cu(110) and Ag(110) surfaces.[14−19] These added row structures exhibit 1D electronic structures, strong correlation in the Cu(Ag)−O chain separations, low coordination of metal atoms that enables high structural flexibility toward interaction with adsorbates, and chemical properties that are intermediate between those of molecules and 2D surfaces.[13,16,20,21] The structure and dimensionality of 1D surfaces necessitates strongly anisotropic interactions, which promotes adsorbate correlation.[13,22] For example, adsorption of one molecule on a 1D chain can promote or poison further adsorption in the proximity of the primary site. Furthermore, adsorbate diffusion can be highly anisotropic, for example restricting the motion predominantly along the 1D chains. In the case of CO chemisorption on Cu(110)-2 × 1-O added row surface, we have shown how the particular properties of 1D molecular chains enable anisotropic 1D self-assembly of CO molecules into molecular grating structures that seemingly contradict the well-established characteristics of CO adsorption on 2D metal surfaces.[13,20,21]

Strongly electron withdrawing organic molecules can extract atoms from metal substrates to self-organize into highly structured surface metal−organic compounds.[23−28] Although 2D metal−organic compounds can have novel interactions with adsorbates,[29] they lack the structural flexibility, which enables 1D MOCs to respond to chemical stimulation.[13] Self-assembled 1D MOCs on 2D single crystalline metal surfaces provide metal adatom and organic adsorption sites for the investigation of interactions with CO_2 molecules using precise surface science tools. We demonstrate a highly responsive and selective supramolecular platform consisting of surface supported 1D metal−organic chains with high flexural and translational degrees-of-freedom for CO_2 capture, by real-space imaging with a low temperature scanning tunneling microscopy (STM) of the molecular scale correlated interactions of CO_2 molecules with the substrate.

The substrates for CO_2 capture are MOCs composed of alternating Au adatom and 1,4-phenylene diisocyanide (PDI) units, $[-Au-PDI-]_n$, self-assembled on single crystal Au surfaces. Figure 1 shows the optimized ball-and-stick structures of an Au−PDI chain assembled on unreconstructed Au(111) surface calculated by density functional theory (DFT). A PDI molecule forms covalent bonds through its carbon atoms of the two equivalent −NC groups to two Au adatoms such that the phenyl ring is parallel to and displaced from the surface and its structure is bent from planar into a *cis*-geometry. The CN− bonds of PDI molecule have predominantly carbene and minor zwitterionic character.[30,31] Pseudohaologen molecules such as PDI are industrially important lixiviants for the extraction of gold from mining ores,[32−34] because of their propensity to form linear polymers with Au atoms. Tysoe and co-workers exploited this characteristic to form and image by STM the linear Au−PDI chains on Au(111) and Au cluster-covered mica surfaces.[35,36] In our experiments, we form Au−PDI chains on both the Au(111) and Au(100) surfaces, and show how they are highly responsive to CO_2 adsorption. Adsorbing CO_2 molecules switch the initially repulsive interaction between Au−PDI chains to attractive causing them to undergo nanometer scale displacement on Au surfaces so that they gather and capture further CO_2 molecules in highly ordered interstitial domains. Thus, CO_2 molecules provoke collective MOC response self-catalyzing their capture. Our study demonstrates that MOC modified metal surfaces could act as platforms for designing the complex physical and chemical interactions for CO_2 capture and reduction.

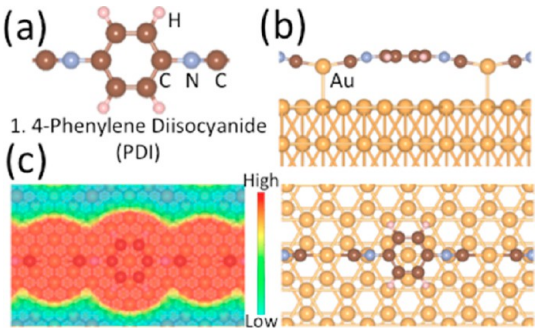

Figure 1. (a) Ball-and-stick model structure of a PDI molecule. (b) The DFT structure of Au−PDI chain on Au(111) surface with side (upper panel) and top view (lower panel). (c) The DFT simulated STM image of a Au−PDI chain on Au(111) surface. The density of states is integrated from E_f to 0.3 eV above E_f. The balls with brown, pink, blue, and golden colors represent C, H, N, and Au, respectively.

RESULTS AND DISCUSSION

Collective Response of MOCs upon CO_2 Adsorption. Figure 2a shows an STM image of the Au(111) surface covered with dispersed Au−PDI chains (bright contrast). Contrast of the herringbone reconstructed Au(111) surface, which is visible beneath the Au−PDI chains, shows that their formation does not lift the surface reconstruction. The chains propagate along three equivalent azimuths (shown with the white arrows) reflecting the 3-fold symmetry of the substrate. They show preference for 1D growth, but the symmetry of the substrate frustrates the long-range 1D propagation due to inevitable collisions among the chains. Consequently, at low coverage the chains have multiple 120° bends, and occasional three-chain junctions.

Within the individual chains, we resolve alternating dim-bright contrast. The inset in Figure 2a shows two repeating units of 1.10 ± 0.05 nm unit length, with each containing an Au adatom and a PDI molecule. We attribute the dim units to gold adatoms because the occasional three chain junctions, such as in Figure 2a,

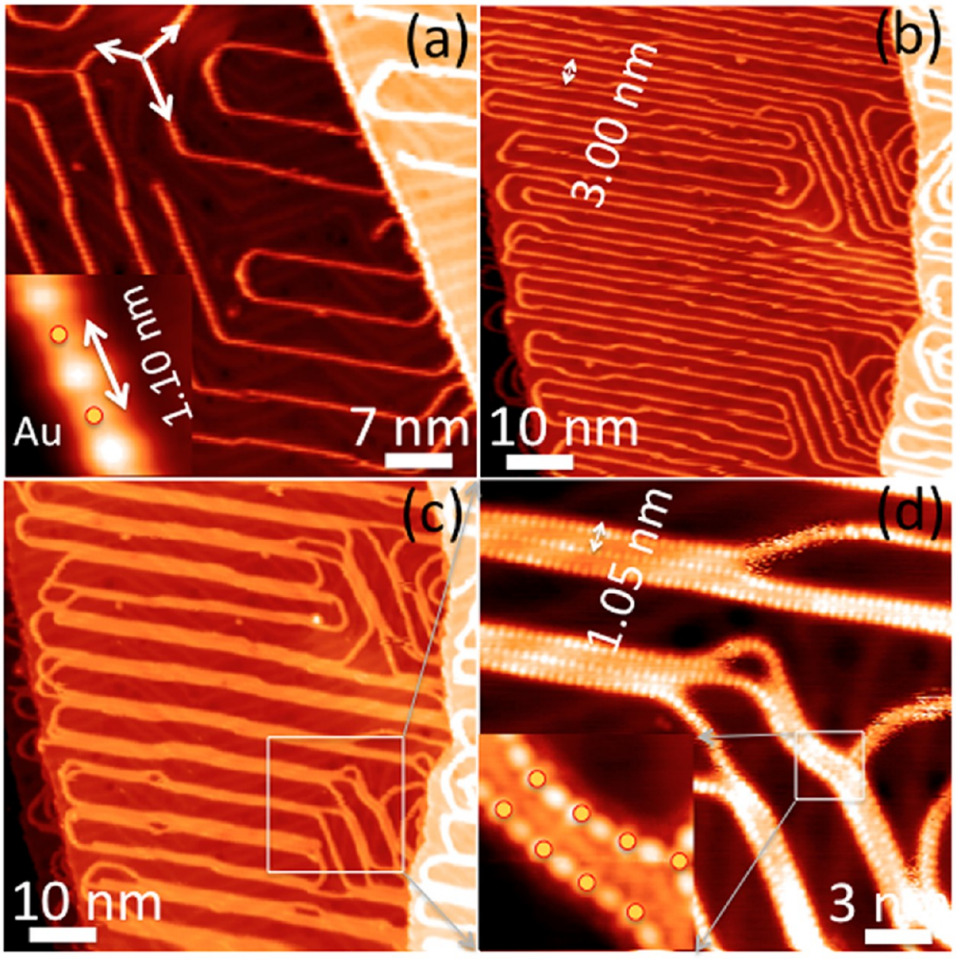

Figure 2. (a) STM image of dispersed Au−PDI chains on Au(111) surface at low coverage. The inset shows the repeating dim-bright contrast within the chains, corresponding to the Au and PDI units, respectively. Au adatoms in the chain are marked with golden dots lined with red color to enhance the contrast. (b and c) STM images of a submonolayer coverage Au−PDI structure. The two images of the same region were acquired before (b) and after (c) CO_2 dosing at 90 K. (d) The magnified image of the square region in (c). The bright contrast between two "coalesced" chains comes from CO_2 molecules confined by them. The inset of (d) shows the additional contrast due to CO_2 molecules captured by the pair of Au−PDI chains.

always occur there: these must be gold adatoms because only they can accept three equivalent bonds to PDI molecules. The bright contrast, therefore, belongs to PDI molecules. This interpretation is in agreement with the DFT calculated structure in Figure 1b and the simulated STM imaging in Figure 1c, where the PDI molecules rise higher above the surface than the Au adatoms and also have a larger footprint.

Figure 2a also shows that the chains grow away from the step edges. Although we are not able to measure the growth process, it is consistent with PDI molecules initially forming a monodentate Au−CN− bond such that the PDI unit projects vertically above the surface. Such bonding of PDI to metal surfaces is frequently invoked based on vibrational spectroscopy and in the context of molecular electronics.[37−40] The monodentate Au−PDI complex can dissociate from step edges and kinks, where the Au atoms are least strongly bound, and diffuse on a terrace until it encounters an Au adatom terminated chain, whereupon its free −NC group can add in the bidentate structure of Figure 1. This process repeats until the chains span the entire terrace. Near the steps, the chains perform a U-turn in order to minimize the number of coordinatively unsaturated monodentate Au adatoms.

The spatial correlation of chains and their relatively uniform spacing for separations as large as 7 nm, *e.g.*, kinks in Figure 2a, can be attributed to a long-range interchain repulsion. The measured work function decrease upon Au−PDI chain formation,[41] as well as DFT calculations, suggests that there is significant charge transfer from the chains to the substrate. Therefore, it is likely that the chains interact through a repulsive dipole−dipole interaction, which favors the uniformly spaced 1D structures.[42−44] The repulsive interaction among the Au−PDI chains is further confirmed by increasing the coverage. With a larger dose of PDI molecules, Figure 2b shows that the Au−PDI chain correlation increases to form domains of parallel lines with a near uniform spacing of ~3.00 nm.

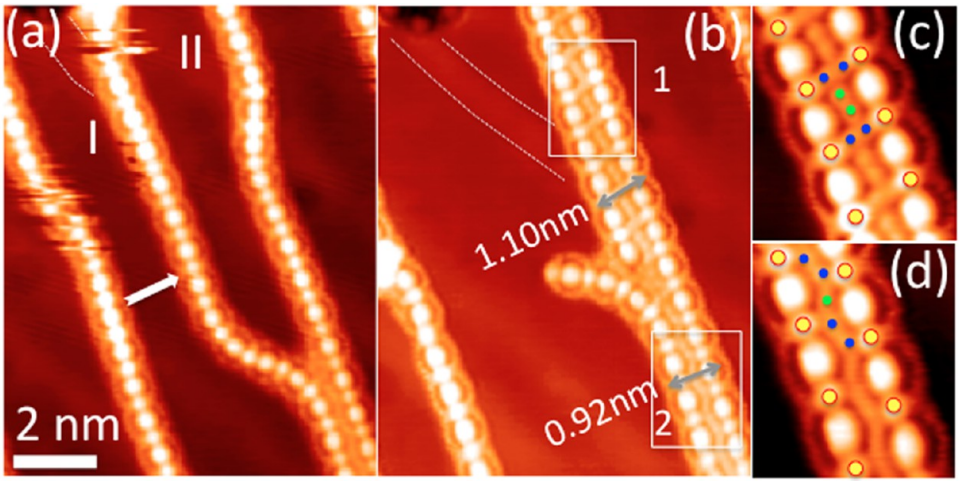

Figure 3. (a and b) STM images, at the same region, of sparse Au−PDI chain covered sample acquired before and after STM tip manipulation. The STM tip nudges chain I along the direction of the white arrow shown in (a). After manipulation, the chain I is broken and moves, exposing the initially partly covered herringbone reconstruction (brighter contrast indicated by the dotted lines). (c and d) High-resolution STM images of the regions indicated by the rectangles 1 and 2 in (b) showing two kinds of CO_2 structures. Au adatoms in the chains, CO_2 molecules interacting directly with Au atoms, and those interacting with PDI molecules are labeled by the golden, deep blue, and green dots, respectively.

Further increasing the dose of PDI molecules increases the chain density continuously, until the minimum average interchain distance saturates at 1.60 ± 0.05 nm (Figure 1 in Supporting Information). This is still wider than the monolayer structure with a minimum distance of 0.5 nm that was reported by Tysoe and coworkers.[35,36] The lower maximum coverage in our work may reflect different preparation conditions, such as the dosing rate. The minimum 1.60 nm spacing at monolayer coverage exceeds the van der Waals distance and therefore is still most likely determined by the electrostatic repulsion.

CO_2 dosing onto Au−PDI chain covered Au(111) surface triggers profound changes in the chain distribution on the surface. Figure 2c shows the consequences of CO_2 adsorption on the surface structure by imaging the same region of Figure 2b after exposure to 0.01 Langmuir of CO_2. Instead of the uniform chain distribution in Figure 2a,b, the Au−PDI chains move laterally over the entire terrace width to join into parallel bundles with a typical interchain distance of 1 nm; the increased local chain density exposes regions of the bare Au(111) surface [darker contrast in Figure 2c] as would be expected if CO_2 transformed the interchain repulsion into attraction. A higher resolution image in Figure 2d reveals bright contrast between the two parallel chains corresponding to individual CO_2 molecules [inset in Figure 2d]. Apparently, the CO_2 adsorption transforms the repulsive interaction into an attractive one, triggering the large-scale motion of Au−PDI chains, and thus gluing them together into tight, highly ordered bundles, where CO_2 molecules constitute the glue. The average distance between the chains before the CO_2-induced coalescence in Figure 2b is larger than typical distances for chemical interactions. Thus, in addition to the short-range chemical interaction, the role of CO_2 molecules must also be to quench the long-range repulsion.

***In Situ* Observation of Self-Catalyzed CO_2 Adsorption on MOCs/Au(111) Surface.** Because CO_2 is introduced into the chamber when the STM tip is retracted, we cannot image the CO_2 induced chain motion. The prompt, large-scale restructuring of Au−PDI chains suggests that their motion on nanometer scale on Au surfaces is facile. The kinetic chain response leaves the surface with many metastable structures, such as the kink in chain I, indicated in Figure 3a, which prevents the chains I and II from coalescing into a lower energy paired structure. The energy barrier to joining chains locked in this metastable structure can be overcome by nudging one with the STM tip. We perform this manipulation by turning off the feedback and lowering the tip so that it is almost touching the surface at the position of the white arrow in Figure 3a. The tip is then scanned perpendicular to chain I nudging it toward II. Following this procedure Figure 3b shows the same two Au−PDI chains, which have coalesced into a tight bundle with the manipulated chain I broken at the kink releasing it to optimize its interaction with chain II.

The manipulation results shown in Figure 3a,b represent a manifestation of the self-catalyzing CO_2 adsorption process. The unpaired Au−PDI chains in Figure 3a after exposure to CO_2 molecules acquire halo structures, which emanate from Au adatoms and encircle the PDI molecules. These halo structures are created by multiple CO_2 molecules, which are in motion on the periphery of the chains, but have the strongest interaction with the Au adatom sites. After the manipulation that creates the line pair, the halo structures remain on the periphery of the coalesced chains [Figure 3b], but in between the chains, we can image round protrusions with ordered structures that

do not belong to Au−PDI chains [Figure 3b]. These protrusions correspond to individual CO_2 molecules in stable, highly ordered, *i.e.*, crystalline, structures, which are stabilized by interactions with the Au−PDI chains as well as among other CO_2 molecules. Apparently, the coalesced chains attracted by CO_2 adsorption create a more stable adsorption or "capture" sites for CO_2 molecules than the single chains, which have not undergone CO_2-induced coalescence. Although we cannot image the self-catalyzed process as an acceleration of the adsorption, the CO_2 adsorption clearly induces a large-scale reconstruction of the 1D chains in order to minimize the surface energy; thus, once the chains start to zipper, with Au−PDI chains being the tape and CO_2 molecules the teeth, into close packed structures, a more thermodynamically stable environment is created for further adsorption.

The correlated interaction between the Au−PDI chains and CO_2 molecules explains the self-catalyzed CO_2 capture. Before adsorption, the Au−PDI chains experience a mutual electrostatic repulsion. The electrostatic environment of single Au−PDI chains attracts CO_2 molecules into the loosely bound halo structures. Single Au−PDI chains thus coordinated with CO_2 no longer repel each other and, therefore, can coalesce into bundles. Thus, the adsorption of CO_2 initiates the chain condensation to create a more favorable potential landscape provided by close packed parallel Au−PDI chains, which force CO_2 into interstitial serried ranks.

The interactions, which contribute to the self-catalyzed capture, probably involve charge transfer to CO_2, as well as between the molecular quadrupoles and the chain dipoles. Apparently, these interactions transform chain repulsion into attraction, *i.e.*, they screen the repulsion. In addition, the corrugated potential in the proximity of Au−PDI chains stabilizes the quadrupole−quadrupole interactions among CO_2. These correlated CO_2−Au−PDI chain and CO_2−CO_2 interactions lead to the self-catalyzed adsorption of CO_2 molecules on the MOC covered Au(111) surface. The precise nature of the interaction between CO_2 molecules and Au adatoms, as well as the Au atoms of the reconstructed surface, is yet unclear and is under investigation by DFT calculations.

Further insight in the self-catalyzed adsorption can be obtained from the analysis of the CO_2 molecule arrangements between the coalesced Au−PDI chains. Figure 3c,d shows high-resolution images of regions indicated by rectangles "1" and "2" in Figure 3b, revealing two kinds of CO_2 structures. In "1", the Au atoms on opposing chains are "in-phase". This enables two CO_2 molecules (labeled by the blue dots) to be sandwiched between in-phase Au adatoms in a linear structure with an interchain distance of $\sim 1.10 \pm 0.05$ nm. Four of such CO_2 molecules form a compartment in which two extra CO_2 molecules (labeled by the green dots) are accommodated in between the PDI molecules *without* direct interaction with the Au sites. In "2", the Au adatoms on the opposing chains are "out-of-phase", and the two CO_2 molecules (blue dots) directly interacting with them are in a kinked arrangement. An additional CO_2 molecule is confined in the available space where it is primarily interacting with the PDI units. The three CO_2 molecules per unit cell are thus arranged in a zig-zag structure with an interchain distance of $\sim 0.92 \pm 0.05$ nm. Either configuration supports two types of adsorbed CO_2 molecules, one that is directly interacting with Au sites, and another that primarily interacts with the PDI sites.

The approximate distance between CO_2 molecules in the serried ranks is 0.4 nm, which is typical of the van der Waals distance in CO_2 clusters.[45] Also, the interaction of CO_2 with PDI is likely to be of the van der Waals or weakly hydrogen bonding type. We note that the imaging of individual CO_2 molecules interacting through the van der Waals interaction on metal surfaces is exceptional. On metal surfaces, single CO_2 molecules have been imaged by STM on Ni(110) surface in a chemisorbed state at 110 K,[46] and in a physisorbed state as an isolated molecule as well as complexes with anthroquinone molecules at 20 K on Cu(111) surfaces.[47] In presence of chemisorbed O atoms, CO_2 readily forms stable carbonate, which has also been imaged by STM.[48,49] At 4.5K on CO_2 molecule covered Au(111) surface we can only image unstable structureless rafts of CO_2 clusters. Thus, the formation of Au−PDI chain bundles, initiated by adsorption of CO_2 molecules on Au sites within the chains, provides an exceptional environment for CO_2 adsorption, which enables molecule-resolved imaging of the CO_2 interactions. Our preliminary calculations at the DFT-D level including the van der Waals forces, however, do not confirm CO_2 chemisorption on Au−PDI chains, and cannot explain their large-scale surface reconstruction. The full understanding of the relevant interactions, in particular between CO_2 and Au, will require further *ab initio* theoretical calculations and spectroscopic characterization.

Self-Catalyzed CO_2 Adsorption on MOCs/Au(100) Surface and Reversible CO_2 Capture and Release. Au−PDI chains with similar characteristics to the Au(111) surface also form on the Au(100) surface. The chain response to CO_2 adsorption shows similar self-catalyzed behavior as that on the Au(111) surface, however, both the chain growth and the response to CO_2 adsorption are surface specific. Figure 4a shows the saturated monolayer coverage of Au−PDI chains on Au(100) surface. The chains grow along [011] azimuths and form a grating structure that covers entire terraces with a $\sim 1.40 \pm 0.05$ nm interchain distance. The interchain repulsion appears to hinder tighter chain compression. At a lower coverage it is evident that the chains (Figure 2 in Supporting Information) reside within troughs formed by the 5×20 reconstruction of the Au(100) surface.[50]

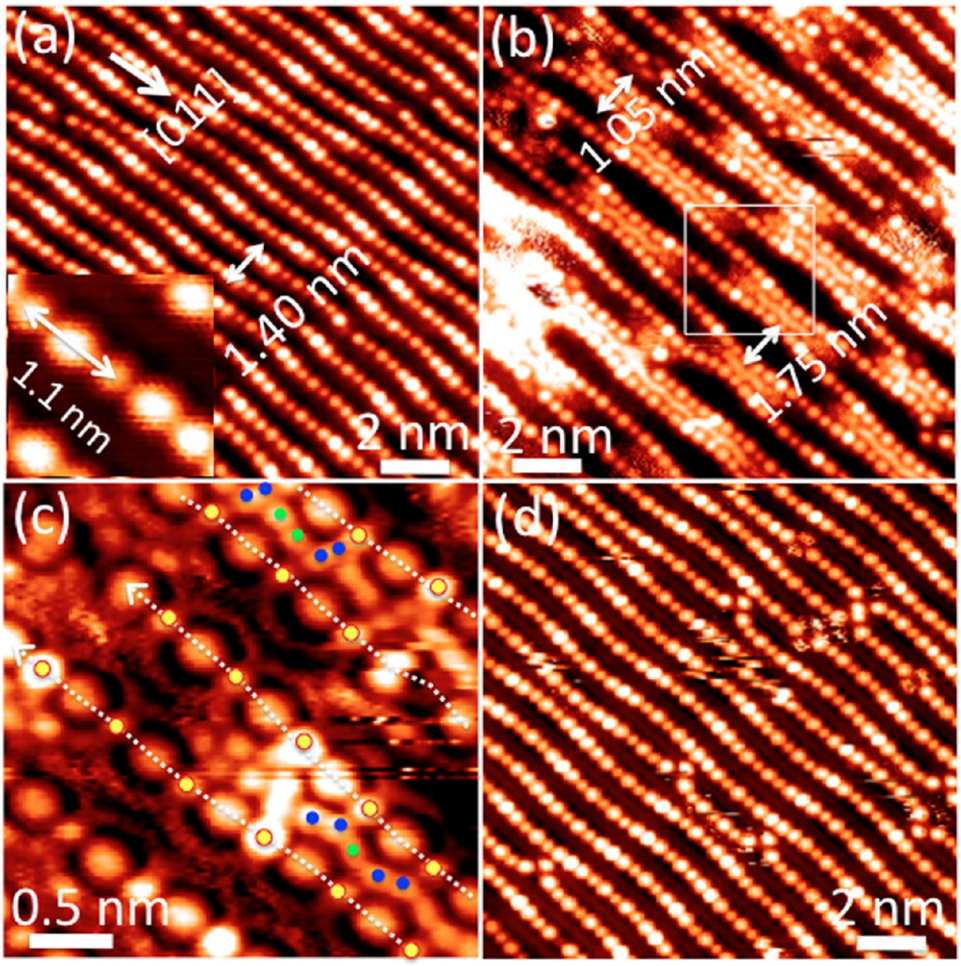

Figure 4. STM images showing CO_2 adsorption and release by Au−PDI chains on Au(100) surface. (a) Uniformly distributed Au−PDI chains at monolayer coverage. The inset shows the dim-bright contrast within the chains. The additional bright contrast with approximately 6 nm periodicity along the chains is consistent with the Au(100) surface reconstruction along [011] azimuth, which modulates the chain height. (b) The same surface after dosing of CO_2 molecules at 90 K. The original grating with nearly uniform spacing is periodically modulated with alternating narrow and wide gaps between the adjacent chains. (c) High-resolution image of the square region in (b) obtained at 0.1 V bias voltage and 0.1 nA current. Two typical CO_2 assembly structures are resolved. (d) Au−PDI chains after desorption of CO_2 molecules. The image in (d) is of the same sample, but not the same location as in (b).

The intertrough distance on the bare Au(100) surface is also about 1.4 nm. Therefore, in the case of Au(100) surface, the corrugation of the substrate probably also has a role in defining the preferential growth direction and the commensurate full monolayer coverage. Within the Au−PDI chains, the alternating dim-bright contrast [inset in Figure 4a] is consistent with the chains on the Au(111) surface. We note that the chains snake across the surface, suggesting that they may be under compressive strain possibly because epitaxial mismatch prevents the optimum registry with the substrate.

Figure 4b shows the consequence of CO_2 adsorption on the surface in Figure 4a. As on the Au(111) surface, there is substantial CO_2 adsorption-induced Au−PDI chain motion; however, the response is characteristic of each surface. On Au(100), the glue of adsorbed CO_2 molecules periodically pulls pairs of chains together on one side and simultaneously pulls them apart on the opposite side. The entire assembly acts as an array of zippers trying to compress against each other. As the zippering occurs on both sides of each chain, the attractive interactions of CO_2 molecules on opposite sides of each Au−PDI chain transform the initially uniform snaking lattice into a tauter periodically modulated one with narrow ($\sim$1.05 $\pm$ 0.05 nm) and wide ($\sim$1.75 $\pm$ 0.05 nm) gaps. It appears that the different responses to CO_2 adsorption of Au−PDI chains on the Au(111) and Au(100) surfaces reflect differences in Au−PDI chain interactions with the substrates. In particular, the 1.4 nm periodicity of the reconstruction on the Au(100) surface may hinder the chain motion over nanometer scale distances and the compressive strain in the chain prevents formation of the close packed parallel chain structures seen on Au(111). The common feature of both surfaces is the CO_2 molecule-induced chain attraction, which elicits the collective Au−PDI chain motion.

The details of the CO_2 molecule−chain interactions can be seen in the high-resolution image Figure 4c, which magnifies the square region in Figure 4b. In the chain constrictions, we see very similar structures as in Figure 3d where the out-of-phase Au−PDI chains trap molecules in a zig-zag structure. The relative chain phase does not seem to be as well-defined as for Au(111) surface, so we also find the CO_2 structures such as observed for the in-phase structures in Figure 3c. As the chain spacing dilates from the narrowest constrictions, STM resolves two-molecule-wide CO_2 ranks. For wider gaps, the contrast becomes fuzzy and the halo structures such as seen in Figure 3a dominate. The larger interchain spacing enables weakly bound CO_2 molecules to exist in a fluctuating state. The similarity of the CO_2−Au−PDI reorganization on the Au(111) and Au(100) surfaces in response to exposure to CO_2 gas suggests that the self-catalyzed adsorption takes place on both surfaces.

We also verified that CO_2 capture can be reversed on both surfaces by heating the samples to room temperature. Figure 4d shows the structure of the annealed CO_2−Au−PDI/Au(100) surface with the CO_2 molecules desorbed and the original Au−PDI superlattice restored, except for some characteristic defects left after CO_2 release. Very similar results are also obtained for the CO_2−Au−PDI on Au(111) surface (Figure 3 in Supporting Information), indicating that the chain responses upon CO_2 adsorption are reversible upon desorption.

Control Experiments. We have performed control experiments and verified that the observed images cannot be due to related species such as CO or carbonate formed by disproportionation of CO_2, as well as impurities in the CO_2 source. Although vibrational spectra of CO interacting with Au−PDI chains on Au(111) surface have been reported,[35] under our experimental conditions, the exposure of Au−PDI chains to CO at 77 K does not affect the chain structure nor can we image adsorbed CO molecules.[51] The stable adsorption of CO on Au−PDI chain covered surface may require higher density coverage than in our work, such as has been reported in ref 35. The oxidation of CO by O atoms adsorbed on Au surfaces is very efficient,[52,53] and therefore, occurrence of the reverse disproportionation is highly unlikely. Therefore, without a source of O atoms,[54,55] carbonate is unlikely to form.

CONCLUSIONS

In summary, by creating 1D metal−organic chains on single crystal gold surfaces, we have discovered unprecedented cooperative behavior induced by CO_2 adsorption. CO_2 molecules interacting with Au−PDI linear polymers with chain lengths in the range of tens of nanometers are able to induce lateral chain motion on nanometer length scales over entire atomically flat substrate terraces. The real-space imaging at the molecular scale reveals the condensation of the metal−organic chains and one molecule wide CO_2 ranks into highly ordered structures exhibiting antithetical behavior to each of those individual materials on gold surfaces. The Au−PDI chains, which normally repel each other, are attracted by the glue of CO_2 molecules. Likewise, CO_2 molecules, which float in loosely bound rafts on Au surfaces, crystallizes into stable and ordered structures that self-catalyze adsorption in the presence of Au−PDI chains. The self-catalyzed adsorption phenomenon reveals the complex physical and chemical interactions that could be harnessed in 3D metal organic frameworks for the purpose of CO_2 capture. The current study can be extended by functionalizing the apparently weakly interacting phenyl group of PDI molecules in order to enhance CO_2 capture and promote its reduction under thermal or electronic stimulation. Our research can be extended to explore other surface supported metal−organic structures,[56−58] which mimic conventional metal−organic nanoporous materials for industrial gas separation.

METHODS

We form supported 1D arrays of MOCs by depositing PDI molecules onto Au(100) and Au(111) surfaces. The samples are prepared at room temperature following the procedure in literature.[35,36,41] After characterizing the surfaces by STM, we dose CO_2 molecules *in situ* at 90 K. STM constant current topographic images are taken at 77 K using a current of 0.05 nA and bias voltage of 0.6 V.

First-principles calculations are carried out using plane-wave basis sets with a cutoff energy of 500 eV using the local density approximation (LDA) known as Ceperley-Alder form (CA),[59] exchange-correlation functional, as implemented in the Vienna *ab initio* simulation package (VASP).[60] The projector augmented wave (PAW) method is used to describe the electron−ion interaction.[61,62] The Au 5d, 6s, H 1s, and 2s, 2p of C, N, O are treated as valence states. A slab model with 6 layers and 4×4 unit cell of Au(111) is used with a vacuum of 20 Å, in order to avoid the interlayer interaction. The energy cutoff is set to 500 eV, and the convergence criteria for energy is 10^{-5} eV; the forces on every ion are relaxed to less than 0.05 eV/Å. During the structure relaxation, $2 \times 2 \times 1$ k-points are adopted, while $8 \times 8 \times 1$ k-points are used to generate the self-consistent wave function and charge density. The DFT-D method is used to incorporate the van der Waals interaction between the PDI−Au chain with the Au(111) surface.[63] The STM image is simulated using an isovalue image based on Tersoff and Hamann's formula and its extension to simulate STM images.[64]

Conflict of Interest: The authors declare no competing financial interest.

Acknowledgment. The authors have benefited from contributions of and discussions with G. Xiang, L. Peker, H. Liu, C. Lin, M. Sterrer, F. Calaza and H.-J. Freund. Some of the calculations were performed in the Environmental Molecular Sciences Laboratory at the PNNL, a user facility sponsored by the DOE Office of Biological and Environmental Research. This research was supported by the Division of Chemical Sciences, Geosciences, and Biosciences, Office of Basic Energy Sciences

of the U.S. Department of Energy through Grant DE-FG02-09ER16056.

Supporting Information Available: Additional results about monolayer MOCs on Au(111) surface, submonolayer MOCs on Au(100) surface, and reversible CO_2 capture and release on MOCs/Au(111) surface. This material is available free of charge *via* the Internet at http://pubs.acs.org.

REFERENCES AND NOTES

1. Jiang, Z.; Xiao, T.; Kuznetsov, V. L.; Edwards, P. P. Turning Carbon Dioxide into Fuel. *Philos. Trans. R. Soc., A* **2010**, *368*, 3343–3364.
2. Mikkelsen, M.; Jorgensen, M.; Krebs, F. C. The Teraton Challenge. A Review of Fixation and Transformation of Carbon Dioxide. *Energy Environ. Sci.* **2010**, *3*, 43–81.
3. Jones, C. W. CO_2 Capture from Dilute Gases as a Component of Modern Global Carbon Management. *Annu. Rev. Chem. Biomol. Eng.* **2011**, *2*, 31–52.
4. Freund, H. J.; Roberts, M. W. Surface Chemistry of Carbon Dioxide. *Surf. Sci. Rep.* **1996**, *25*, 225–273.
5. D'Alessandro, D. M.; Smit, B.; Long, J. R. Carbon Dioxide Capture: Prospects for New Materials. *Angew. Chem., Int. Ed.* **2010**, *49*, 6058–6082.
6. Yaghi, O. M.; O'Keeffe, M.; Ockwig, N. W.; Chae, H. K.; Eddaoudi, M.; Kim, J. Reticular Synthesis and the Design of New Materials. *Nature* **2003**, *423*, 705–714.
7. Li, J. R.; Kuppler, R. J.; Zhou, H. C. Selective Gas Adsorption and Separation in Metal-Organic Frameworks. *Chem. Soc. Rev.* **2009**, *38*, 1477–1504.
8. Li, J. R.; Sculley, J.; Zhou, H. C. Metal-Organic Frameworks for Separations. *Chem. Rev.* **2012**, *112*, 869–932.
9. Sumida, K.; Rogow, D. L.; Mason, J. A.; McDonald, T. M.; Bloch, E. D.; Herm, Z. R.; Bae, T.-H.; Long, J. R. Carbon Dioxide Capture in Metal−Organic Frameworks. *Chem. Rev.* **2011**, *112*, 724–781.
10. Uzun, A.; Keskin, S. Site Characteristics in Metal Organic Frameworks for Gas Adsorption. *Prog. Surf. Sci.* **2014**, *89*, 56–79.
11. Sato, H.; Kosaka, W.; Matsuda, R.; Hori, A.; Hijikata, Y.; Belosludov, R. V.; Sakaki, S.; Takata, M.; Kitagawa, S. Self-Accelerating CO Sorption in a Soft Nanoporous Crystal. *Science* **2014**, *343*, 167–170.
12. Walton, K. S. Metal-Organic Frameworks: Recognizing the Unrecognizable. *Nat. Chem.* **2014**, *6*, 277–278.
13. Feng, M.; Lin, C.; Zhao, J.; Petek, H. Orthogonal Intermolecular Interactions of CO Molecules on a One-Dimensional Substrate. *Annu. Rev. Phys. Chem.* **2012**, *63*, 201–224.
14. Ertl, G. Untersuchung von oberflächenreaktionen mittels beugung langsamer elektronen (LEED): I. Wechselwirkung von O_2 und N_2O mit (110)-, (111)- und (100)-Kupfer-Oberflächen. *Surf. Sci.* **1967**, *6*, 208–232.
15. Kern, K.; Niehus, H.; Schatz, A.; Zeppenfeld, P.; Goerge, J.; Comsa, G. Long-Range Spatial Self-Organization in the Adsorbate-Induced Restructuring of Surfaces: Cu{110}-(2 x1)O. *Phys. Rev. Lett.* **1991**, *67*, 855.
16. Taniguchi, M.; Tanaka, K.-i.; Hashizume, T.; Sakurai, T. Ordering of Ag−O chains on the Ag(110) Surface. *Surf. Sci.* **1992**, *262*, L123–L128.
17. Hartmann, N.; Madix, R. J. Dynamical Rearrangements of the (2 × 1)O Adlayer during CO Oxidation on Cu(110). *Surf. Sci.* **2002**, *516*, 230–236.
18. Nakagoe, O.; Watanabe, K.; Takagi, N.; Matsumoto, Y. Role of Structural Fluctuation in a Surface Reaction Studied by Scanning Tunneling Microscopy: The CO + O → CO_2 Clean-Off Reaction on Ag(110)-(2 × 1)-O. *Phys. Rev. Lett.* **2003**, *90*, 226105.
19. Tanaka, K.-i. Surface Nano-Structuring by Adsorption and Chemical Reactions. *Materials* **2010**, *3*, 4518–4549.
20. Feng, M.; Cabrera-Sanfelix, P.; Lin, C.; Arnau, A.; Sánchez-Portal, D.; Zhao, J.; Echenique, P. M.; Petek, H. Orthogonal Interactions of CO Molecules on a One-Dimensional Substrate. *ACS Nano* **2011**, *5*, 8877–8883.
21. Lin, C.; Feng, M.; Zhao, J.; Cabrera-Sanfelix, P.; Arnau, A.; Sánchez-Portal, D.; Petek, H. Theory of Orthogonal Interactions of CO Molecules on a One-Dimensional Substrate. *Phys. Rev. B* **2012**, *85*, 125426.
22. Feng, M.; Lee, J.; Zhao, J.; Yates; Petek, H. Nanoscale Templating of Close-Packed C_{60} Nanowires. *J. Am. Chem. Soc.* **2007**, *129*, 12394–12395.
23. Maksymovych, P.; Voznyy, O.; Dougherty, D. B.; Sorescu, D. C.; Yates, J. T., Jr. Gold Adatom as a Key Structural Component in Self-Assembled Monolayers of Organosulfur Molecules on Au(111). *Prog. Surf. Sci.* **2010**, *85*, 206–240.
24. Bartels, L. Tailoring Molecular Layers at Metal Surfaces. *Nat. Chem.* **2010**, *2*, 87–95.
25. Röckert, M.; Ditze, S.; Stark, M.; Xiao, J.; Steinrück, H.-P.; Marbach, H.; Lytken, O. Abrupt Coverage-Induced Enhancement of the Self-Metalation of Tetraphenylporphyrin with Cu(111). *J. Phys. Chem. C* **2013**, *118*, 1661–1667.
26. Klappenberger, F. Two-Dimensional Functional Molecular Nanoarchitectures—Complementary Investigations with Scanning Tunneling Microscopy and X-ray Spectroscopy. *Prog. Surf. Sci.* **2014**, *89*, 1–55.
27. Shchyrba, A.; Wäckerlin, C.; Nowakowski, J.; Nowakowska, S.; Björk, J.; Fatayer, S.; Girovsky, J.; Nijs, T.; Martens, S. C.; Kleibert, A.; Stöhr, M.; Ballav, N.; Jung, T. A.; Gade, L. H. Controlling the Dimensionality of On-Surface Coordination Polymers *via* Endo- or Exoligation. *J. Am. Chem. Soc.* **2014**, *136*, 9355–9363.
28. Otero, R.; Gallego, J. M.; de Parga, A. L. V.; Martín, N.; Miranda, R. Molecular Self-Assembly at Solid Surfaces. *Adv. Mater.* **2011**, *23*, 5148–5176.
29. Cheng, Z.; Wyrick, J.; Luo, M.; Sun, D.; Kim, D.; Zhu, Y.; Lu, W.; Kim, K.; Einstein, T. L.; Bartels, L. Adsorbates in a Box: Titration of Substrate Electronic States. *Phys. Rev. Lett.* **2010**, *105*, 066104.
30. Ramozzi, R.; Cheron, N.; Braida, B.; Hiberty, P. C.; Fleurat-Lessard, P. A Valence Bond View of Isocyanides' Electronic Structure. *New J. Chem.* **2012**, *36*, 1137–1140.
31. Wang, X.-B.; Wang, Y.-L.; Yang, J.; Xing, X.-P.; Li, J.; Wang, L.-S. Evidence of Significant Covalent Bonding in $Au(CN)_2^-$. *J. Am. Chem. Soc.* **2009**, *131*, 16368–16370.
32. Hakala, M. O.; Pyykko, P. Gold as Intermolecular Glue: A Predicted Planar Triaurotriazine, $C_3Au_3N_3$, Isomer of Gold Cyanide. *Chem. Commun.* **2006**, *0*, 2890–2892.
33. Katz, M. J.; Sakai, K.; Leznoff, D. B. The Use of Aurophilic and Other Metal-Metal Interactions as Crystal Engineering Design Elements To Increase Structural Dimensionality. *Chem. Soc. Rev.* **2008**, *37*, 1884–1895.
34. Samanta, D.; Wu, M. M.; Jena, P. $Au(CN)_n$ Complexes: Superhalogens with Pseudohalogen as Building Blocks. *Inorg. Chem.* **2011**, *50*, 8918–8925.
35. Boscoboinik, J.; Kestell, J.; Garvey, M.; Weinert, M.; Tysoe, W. T. Creation of Low-Coordination Gold Sites on Au(111) Surface by 1,4-Phenylene Diisocyanide Adsorption. *Top. Catal.* **2011**, *54*, 20–25.
36. Kestell, J.; Abuflaha, R.; Boscoboinik, J. A.; Bai, Y.; Bennett, D. W.; Tysoe, W. T. Linking Gold Nanopartilces with Conductive 1,4-Phenylene Diiscocyanide-Gold Oligomers. *Chem. Commun.* **2013**, *49*, 1422–1424.
37. Hong, S.; Reifenberger, R.; Tian, W.; Datta, S.; Henderson, J. I.; Kubiak, C. P. Molecular Conductance Spectroscopy of Conjugated, Phenyl-Based Molecules on Au(111): The Effect of End Groups on Molecular Conduction. *Superlattices Microstruct.* **2000**, *28*, 289–303.
38. Dupraz, C. J. F.; Beierlein, U.; Kotthaus, J. P. Low Temperature Conductance Measurements of Self-Assembled Monolayers of 1,4-Phenylene Diisocyanide. *ChemPhysChem* **2003**, *4*, 1247–1252.
39. Angelici, R. J.; Lazar, M. Isocyanide Ligands Adsorbed on Metal Surfaces: Applications in Catalysis, Nanochemistry, and Molecular Electronics. *Inorg. Chem.* **2008**, *47*, 9155–9165.
40. Swanson, S. A.; McClain, R.; Lovejoy, K. S.; Alamdari, N. B.; Hamilton, J. S.; Scott, J. C. Self-Assembled Diisocyanide Monolayer Films on Gold and Palladium. *Langmuir* **2005**, *21*, 5034–5039.
41. Zhou, J.; Acharya, D.; Camillone, N.; Sutter, P.; White, M. G. Adsorption Structures and Electronic Properties of

1,4-Phenylene Diisocyanide on the Au(111) Surface. *J. Phys. Chem. C* **2011**, *115*, 21151–21160.
42. Vanderbilt, D. Phase Segregation and Work-Function Variations on Metal Surfaces: Spontaneous Formation of Periodic Domain Structures. *Surf. Sci.* **1992**, *268*, L300–L304.
43. Zeppenfeld, P.; Krzyzowski, M.; Romainczyk, C.; Comsa, G.; Lagally, M. G. Size Relation for Surface Systems with Long-Range Interactions. *Phys. Rev. Lett.* **1994**, *72*, 2737–2740.
44. Fratesi, G. Depolarization and Bonding in Quasi-One-Dimensional Na Structures on Cu(001). *Phys. Rev. B* **2011**, *84*, 155424.
45. Weida, M. J.; Sperhac, J. M.; Nesbitt, D. J. High-Resolution Infrared Diode Laser Spectroscopy of $(CO_2)_3$: Vibrationally Averaged Structures, Resonant Dipole Vibrational Shifts, and Tests of CO_2-CO_2 Pair Potentials. *J. Chem. Phys.* **1995**, *103*, 7685–7699.
46. Dri, C.; Peronio, A.; Vesselli, E.; Africh, C.; Rizzi, M.; Baldereschi, A.; Peressi, M.; Comelli, G. Imaging and Characterization of Activated CO_2 Species on Ni(110). *Phys. Rev. B* **2010**, *82*, 165403.
47. Wong, K. L.; Pawin, G.; Kwon, K. Y.; Lin, X.; Jiao, T.; Solanki, U.; Fawcett, R. H. J.; Bartels, L.; Stolbov, S.; Rahman, T. S. A Molecule Carrier. *Science* **2007**, *315*, 1391–1393.
48. Okawa, Y.; Tanaka, K.-i STM Investigation of the Reaction of Ag-O Added Rows with CO_2 on a Ag(110) Surface. *Surf. Sci.* **1995**, *344*, L1207–L1212.
49. Guo, X.-C.; Madix, R. J. $CO_2 + O$ on Ag(110): Stoichiometry of Carbonate Formation, Reactivity of Carbonate with CO, and Reconstruction-Stabilized Chemisorption of CO_2. *J. Phys. Chem. B* **2001**, *105*, 3878–3885.
50. Ercolessi, F.; Tosatti, E.; Parrinello, M. Au (100) Surface Reconstruction. *Phys. Rev. Lett.* **1986**, *57*, 719–722.
51. Maksymovych, P.; Yates, J. T., Jr. Unexpected Spontaneous Formation of CO Clusters on the Au(111) Surface. *Chem. Phys. Lett.* **2006**, *421*, 473–477.
52. Schubert, M. M.; Hackenberg, S.; van Veen, A. C.; Muhler, M.; Plzak, V.; Behm, R. J. CO Oxidation over Supported Gold Catalysts—"Inert" and "Active" Support Materials and Their Role for the Oxygen Supply during Reaction. *J. Catal.* **2001**, *197*, 113–122.
53. Lopez, N.; Janssens, T. V. W.; Clausen, B. S.; Xu, Y.; Mavrikakis, M.; Bligaard, T.; Nørskov, J. K. On the Origin of the Catalytic Activity of Gold Nanoparticles for Low-Temperature CO Oxidation. *J. Catal.* **2004**, *223*, 232–235.
54. Gong, J. L.; Mullins, C. B. Surface Science Investigations of Oxidative Chemistry on Gold. *Acc. Chem. Res.* **2009**, *42*, 1063–1073.
55. Burghaus, U. Surface Chemistry of CO_2—Adsorption of Carbon Dioxide on Clean Surfaces at Ultrahigh Vacuum. *Prog. Surf. Sci.* **2014**, *89*, 161–217.
56. Makiura, R.; Motoyama, S.; Umemura, Y.; Yamanaka, H.; Sakata, O.; Kitagawa, H. Surface Nano-Architecture of a Metal-Organic Framework. *Nat. Mater.* **2010**, *9*, 565–571.
57. Colson, J. W.; Woll, A. R.; Mukherjee, A.; Levendorf, M. P.; Spitler, E. L.; Shields, V. B.; Spencer, M. G.; Park, J.; Dichtel, W. R. Oriented 2D Covalent Organic Framework Thin Films on Single-Layer Graphene. *Science* **2011**, *332*, 228–231.
58. Wang, Z.; Liu, J.; Lukose, B.; Gu, Z.; Weidler, P. G.; Gliemann, H.; Heine, T.; Wöll, C. Nanoporous Designer Solids with Huge Lattice Constant Gradients: Multiheteroepitaxy of Metal−Organic Frameworks. *Nano Lett.* **2014**, *14*, 1526–1529.
59. Ceperley, D. M.; Alder, B. J. Ground State of the Electron Gas by Stochastic Method. *Phys. Rev. Lett.* **1980**, *45*, 566–569.
60. Kresse, G.; Furthmüller, J. Effective Iterative Schemes for *ab Initio* Total-Energy Calculations Using a Plane-Wave Basis Set. *Phys. Rev. B* **1996**, *54*, 11169–11186.
61. Blöchl, P. E. Projector Augmented-Wave Method. *Phys. Rev. B* **1994**, *50*, 17953–17979.
62. Kresse, G.; Joubert, D. From Ultrasoft Pseudopotentials to the Projector Augumented-Wave Method. *Phys. Rev. B* **1999**, 59.
63. Grimme, S. Semiempirical GGA-type Density Functional Constructed with a Long-Range Dispersion Correction. *J. Comput. Chem.* **2006**, *27*, 1787–1799.
64. Tersoff, J.; Hamann, D. R. Theory of the Scaning Tunneling Microscope. *Phys. Rev. B* **1985**, *31*, 805–813.